NUMERICAL MODEL AND EXPERIMENTAL VALIDATION OF THE HEAT TRANSFER IN AIR COOLED SOLAR PHOTOVOLTAIC PANEL

by

Senthil Kumar RANGANATHAN [a*], Natarajan ELUMALAI [b], and Puja Priyadharshini NATARAJAN [c]

[a] Department of Mechanical Engineering, Institute for Energy Studies, Anna University, Chennai, India
[b] Department of Mechanical Engineering, KCG College of Technology, Chennai, India

In this paper, a meticulous numerical model is developed and simulated using computational fluid dynamics technique so as to analyse the heat transfer and temperature distribution on each layer of the air cooled solar photovoltaic panel. The proposed numerical model comprises of bottom air cooling layer and diverse layers of solar panel such as glass, ethyl vinyl acetate, photovoltaic cell, and tedlar. The discrete ordinates model is employed to apply the solar load in the numerical computation. The computational fluid dynamics simulated average temperatures are compared with the experimental measured values and found to be in commendable agreement. The $RMSE_1$, $RMSE_2$, and R-squared values were obtained for top glass, tedlar and outlet air temperature is 1.112949, 0.022619, 0.998175, 0.993115, 0.019556, 0.998451, and 0.077683, 0.022618, 0.988113, respectively. The top glass and photovoltaic cell contour clearly visuvalizes the temperature distribution through out the layer. It is also found that the maximum top glass, photovoltaic cell, tedlar and outlet air temperature of photovoltaic-thermal system are about 58.06 °C, 58.39 °C, 59.44 °C, and 45.48 °C, respectively.

Key words: *photovoltaic-thermal, temperature distribution, CFD simulation, heat transfer*

Introduction

Solar photovoltaic-thermal (PV/T) systems convert solar irradiation into electrical and thermal energy. These systems serve as dual energy extraction mode; the photovoltaic (PV) cell, which converts photons in the solar radiation into electricity and the solar thermal collector, which absorbs the waste heat energy from the PV module. The PV module temperature increases the electrical resistance of the PV cell increases which leads to decrease in electrical efficiency of the PV cell. Solar thermal collectors can be designed to absorb the heat from the PV panel thereby cooling the cells and thus electrical efficiency is increased by decreasing the electrical resistance. This result's a cool operating PV panel with higher potency and longer life and therefore the extracted hot air which will be used for domestic and industrial applications. The decrease in electrical efficiency of every degree rise in temperature for monocrystalline and polycrystalline is about 0.45%. In case of amorphous silicon cells the decrease in electrical effi-

---

S1072

Ranganathan, S. K., *et al.*: Numerical Model and Experimental Validation of the Heat ...
THERMAL SCIENCE: Year 2016, Vol. 20, Suppl. 4, pp. S1071-S1081

ciency per degree rise in temperature is about 0.25%. This unwanted loss is minimized by using a proper fluid circulation cooling methods [1]. The effects of air flow rate and the performance of absorber plate and PV cells have been examined on PV/T air collector in four different models under same climate conditions. The energy balance equation for each models are solved numerically and evaluate the thermal and electrical performances [2]. The theoretical analysis with experimental results are validated for PV module integrated with air duct and found that the increase in overall thermal efficiency of the system is about 18% due to utilization of thermal energy from PV module [3]. The dual cooling PV/T collector using water and air as a heat extraction fluid are experimentally analyzed and achieved the satisfactory electrical and thermal efficiency [4]. Integrated PV and solar air collector system is developed and the theoretically obtained results are experimentally validated. They have indicated that PV module temperature are controlled and reduced in consequence of adjusting the mass flow of air in solar collector and therefore the efficiency of PV module are often enhanced [5]. The experimentally validated CFD model of a completely unique building integrated PV/T collector was analyzed and the effect of active heat recovery on cell efficiency was studied. Thermal and overall efficiencies of the system reached 19% and 34.9%, respectively [6]. The electrical and thermal parameters of a solar PV/T air collector was simulated by the use of computer simulation program. It is conjointly found that the overall energy, thermal and electrical efficiency of solar PV/T air collector is about 45%, 17.18%, and 10.01%, respectively, for a given climatic, operating, and design parameters [7]. The optimum electrical and thermal arrangements of hybrid PV/T collectors are studied and found the increase in temperature of the PV cells affect the electrical performance of the system. Also the electrical efficiency of each PV cell may vary due to the temperature gradient exists along the absorber. In order to evaluate the solar cell temperature distribution, the thermal analysis has been carried out by using CFD software [8]. The analytical expression for semi-transparent and opaque type building integrated PV/T collector in façade and roof modes are developed. The difference is room temperature for facade and roof mode with air cooling duct is 1.46 °C and 1.13 °C, respectively. Also the difference is room temperature for façade and roof mode without air cooling duct is 9.80 °C and 9.55 °C, respectively. In addition, the increase in mass flow rate of air increases the heat transfer rate between the PV module and flowing air [9]. A multiphysics model that is capable of estimating the 3-D structural and thermal performance in addition to the electrical performance of a PV module under given environmental conditions are developed. The thermal, structural, and electrical performance of a PV module has been analyzed for four different environmental condition days under without and with cooling modes [10]. The heat transfers and fluid flow in solar air heater was numerically studied using CFD technique. The RNG k-ε turbulence model is used to solve the computational domain. The output numerical results are validated with similar available literature experimental values and found to be in good agreement with them [11].The electrical and thermal performance of the air based solar PV/T system are experimentally examined and the results shows the thermal and electrical efficiency of air cooled PV/T system is 22% and 15%, respectively [12]. The performance of air based hybrid PV/T collectors in four different models via; no cooling, single duct double pass air, double duct single pass air, and single duct single pass air are evaluated experimentally and theoretically. The results show the single duct single pass gives higher electrical efficiency [13]. In the present work, fluid flow analysis and temperature distribution on solar panel has been scientifically carried out by experimental method and CFD technique. The results obtained by CFD simulation are validated with experimental results. The root mean square errors (RMSE) and R-squared values are computed for the top glass, tedlar, and the outlet air temperature.

Ranganathan, S. K., *et al.*: Numerical Model and Experimental Validation of the Heat ...
THERMAL SCIENCE: Year 2016, Vol. 20, Suppl. 4, pp. S1071-S1081

S1073

The CFD simulation

Governing equations

The heat transfer in air cooled PV/T system involves a fluid and multiple solid domains. The fluid domain covers the working fluid inside the air duct. The solid domain consists of each material layer (top glass, ethyl vinyl acetate – EVA, PV cell, tedlar) in the PV panel. The heat transfer equations for solid and fluid domain are given by eqs. (1) and (2), respectively [14]:

$$\rho_i C_{p,i} \frac{\partial T_i(x, y, z)}{\partial t} = \nabla(q_i) + Q_i \quad i = 1, 2, \dots n \tag{1}$$

$$\rho C_p \frac{\partial T}{\partial t} + \rho C_p u \nabla T(x, y, z) = \nabla(q) + Q_{vh} \tag{2}$$

where

$$q = k_{cond} \nabla T \tag{3}$$

The equation of momentum and continuity governing the fluid flow inside the air duct are given by eqs. (4) and (5) [15]:

$$\rho \frac{\partial u}{\partial t} + \rho(u\nabla)u = \nabla\left[-p\mathrm{I} + (\mu + \mu_T)(\nabla u + \nabla u^T) - \frac{2}{3}\rho k\mathrm{I}\right] \tag{4}$$

$$\rho \nabla u = 0 \tag{5}$$

The k-ε turbulence model used in the CFD analysis is given eqs. (6)-(8) [16].

$$\frac{\partial}{\partial t}(\rho k) + \frac{\partial}{\partial x_i}(\rho k u_i) = \frac{\partial}{\partial x_j}\left[\left(\mu + \frac{\mu_t}{\sigma_k}\right)\frac{\partial k}{\partial x_j}\right] + G_k + G_b - \rho\varepsilon - Y_M + S_k \tag{6}$$

$$\frac{\partial}{\partial t}(\rho\varepsilon) + \frac{\partial}{\partial x_i}(\rho\varepsilon u_i) = \frac{\partial}{\partial x_j}\left[\left(\mu + \frac{\mu_t}{\sigma_\varepsilon}\right)\frac{\partial\varepsilon}{\partial x_j}\right] + C_{1\varepsilon}\frac{\varepsilon}{k}(G_k + G_{3\varepsilon}G_b) - C_{2\varepsilon}\rho\frac{\varepsilon^2}{k} + S_\varepsilon \tag{7}$$

In eqs. (6) and (7), G_k represents the turbulence kinetic energy caused by the mean velocity gradients, G_b – the generation of turbulence kinetic energy due to the buoyancy, Y_M – the unsteady dilatation in compressible turbulence to the overall dissipation rate, $C_{1\varepsilon}$, $C_{2\varepsilon}$, $C_{3\varepsilon}$ are constants values. The turbulent Prandtl numbers for k and ε is represented by σ_k and σ_ε, respectively, S_k and S_ε are user-defined source terms.

The eddy (or turbulent) viscosity, μ_t is calculated by combining k and ε and is defined by eq. (8) [16]:

$$\mu_t = \rho C_\mu \frac{k^2}{\varepsilon} \tag{8}$$

where C_μ is constant value. The other model constant values are $C_{1\varepsilon} = 1.44$, $C_{2\varepsilon} = 1.92$, $\sigma_k = 1.0$, and $\sigma_\varepsilon = 1.3$ (FLUENT).

The discrete ordinates (DO) radiation model is used to apply the incoming solar radiation into the computational domain. The DO radiative transfer equation in the direction $\vec{s}$ as a field equation and radiative transfer equation for spectral intensity $I_\lambda(\vec{r}, \vec{s})$ are given by eqs. (9) and (10) [16]:

$$\nabla[I(\vec{r}, \vec{s})\vec{s}] + (a + \sigma_s)I(\vec{r}, \vec{s}) = an^2 \frac{\sigma T^4}{\pi} + \frac{\sigma_s}{4\pi}\int_0^{4\pi} I(\vec{r}, \vec{s}')\Phi(\vec{s}, \vec{s}')\,\mathrm{d}\Omega' \tag{9}$$

$$\nabla[I_\lambda(\vec{r},\vec{s})\vec{s}] + (a_\lambda + \sigma_s)I_\lambda(\vec{r},\vec{s}) = a_\lambda n^2 I_{b\lambda} + \frac{\sigma_s}{4\pi}\int_0^{4\pi} I_\lambda(\vec{r},\vec{s}')\Phi(\vec{s},\vec{s}')\,\mathrm{d}\Omega' \tag{10}$$

where λ is the wave length, a_λ – the co-efficient of spectral absorption, and $I_{b\lambda}$ – the intensity of black body given by the planck function. The other parameters such as scattering phase function (σ_s), scattering coefficient (Φ) and the refractive index (n) are assumed independent of wave-length.

The coupling between energy and radiation intensities at a cell (known as COMET) accelerates the convergence of the finite volume scheme for radiative heat transfer. The discrete energy equation for coupled method when integrated over a control volume i and is defined by eqs. (11) [16]:

$$\sum_{j=1}^{N}\mu_{ij}^{T}T_j - \beta_i^T T_i = \alpha_i^T \sum_{k=1}^{L} I_i^k \omega_k - S_i^T + S_i^h \tag{11}$$

where

$$\alpha_i^T = k\Delta V_i \tag{12}$$

$$\beta_i^T = 16k\sigma T_i^{*3}\Delta V_i \tag{13}$$

$$S_i^T = 12k\sigma T_i^{*4}\Delta V_i \tag{14}$$

where ΔV and k are the control volume and co-efficient of absorption, respectively. The coefficient μ_{ij}^T and the source term S_i^h are owing to the discretization of the diffusion and convection terms as well as the non-radiative source terms.

Computational domain

The 3-D computational domain of solar PV/T system was modelled using ANSYS geometric modelling tool. It consists of five solid layers: (glass, EVA, PV cell, bottom EVA, tedlar) and one fluid layer (air domain). Computational domain of PV/T system used in the present numerical simulation is shown in fig. 1. Table 1 shows the geometrical dimensions of solar PV/T system used in the CFD simulation.
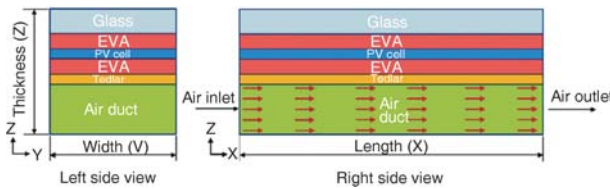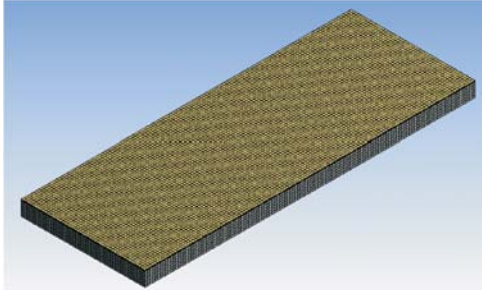

Figure 1. Computational domain of PV/T system

Table 1. Geometrical dimensions of PV/T system

Name	Dimensions
Glass layer	$1.2 \times 0.527 \times 0.003$
EVA layer	$1.2 \times 0.527 \times 0.0005$
PV cell layer	$1.2 \times 0.527 \times 0.0003$
Tedlar layer	$1.2 \times 0.527 \times 0.0005$
Air path layer	$1.2 \times 0.527 \times 0.03$

Grid generation

The grid generation is performed by using ANSYS ICEM CFD. The good quality mesh is achieved by employing hexahedral elements of fine size and patch conforming technique. The number of nodes and elements are found to be 752136 and 712800, respectively. The final meshoutput of PV/T domain is shown in fig. 2. Grid generation settings used in the present simulation is given in tab. 2.

Ranganathan, S. K., *et al.*: Numerical Model and Experimental Validation of the Heat ...
THERMAL SCIENCE: Year 2016, Vol. 20, Suppl. 4, pp. S1071-S1081

S1075

Figure 2. Mesh output of PV/T domain

Table 2. Grid generation settings

Name	Option/value
Element	Hexahedral
Method	Patch conforming
Relevance centre	Fine
No. of elements	71500
No. of nodes	80172

Simulation assumptions

The heat transfers and temperature distribution of the solar PV/T panel is carried out by assuming the following assumptions:
–   all the material properties used in the simulation is to be isotropic and independent of temperature,
–   the electrical bus bar and fingers of solar panel are neglected in the computational domain for simplicity,
–   the computational domain side walls are taken to be adiabatic,
–   the ambient temperature is equal on every area exposed to the environment,
–   the reference temperature and pressure is 25 °C and 101325 Pa,
–   solar radiation is not reflected to any surface is fully transmitted to the layer below,
–   the flow is steady, turbulent, and 3-D,
–   the operating fluid (air) is assumed to be incompressible,
–   no-slip boundary condition is assigned to the walls in contact with the fluid in the model, and
–   the steady-state conditions are performed.

Boundary conditions and set-up

Suitable boundary conditions were impressed on the computational domain, as per the physics of the problem. The thermo-physical properties of air and solar panel materials are assumed to be constant. Inlet and outlet boundary condition was applied as velocity inlet and pressure outlet condition, respectively. Solid and fluid regions are bounded by wall boundary conditions.Due to existence of no-slip and impermeability, the velocity components at the wall were set to zero. A solar insolation is applied at the top surface of the glass using do-radiation. The bottom and side surfaces of the solar PV/T system are defined as wall with zero heat flux condition to effect insulated conditions. The SIMPLE scheme was used to couple the pressure-velocity in the computation and the convection terms are discretized by using second order upwind scheme. The minimum convergence criterion for continuity, velocity and turbulence equations was 10^{-5}, for energy and do-intensity equation was 10^{-6}. The various thermo-physical material properties used in CFD analysis is shown in tab. 3.

Validation of CFD results

To validate the present CFD analysis of PV/T system, the series of experiment tests was conducted under two different modes. Mode1: without cooling of PV panel, Mode 2: the PV panel is cooled by forced air. The experiment was conducted in the Institute for Energy Studies, Anna University (Chennai, India, 13.0827° N, 80.2707° E) and the experiment rig is shown

S1076

Ranganathan, S. K., *et al.*: Numerical Model and Experimental Validation of the Heat ...
THERMAL SCIENCE: Year 2016, Vol. 20, Suppl. 4, pp. S1071-S1081

Table 3. Thermo-physical material properties

Material	Tempered glass	EVA	Silicon	Tedlar
Layer	Top cover	Encapsulent	PV cell	Bottom cover
Thermal conductivity [$Wm^{-1}K^{-1}$]	2	0.311	130	0.15
Specific heat capacity [$Jkg^{-1}K^{-1}$]	500	2090	677	1250
Density [kgm^{-3}]	2450	950	2330	1200
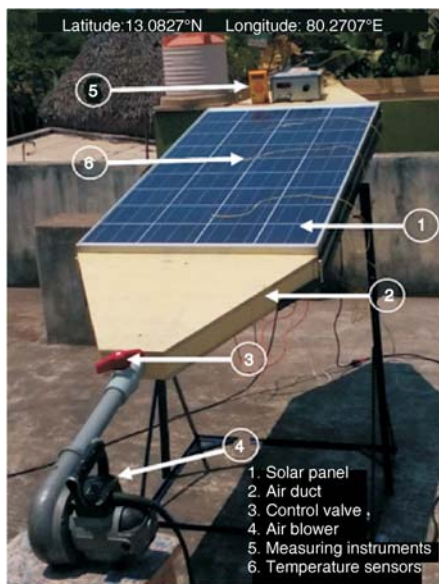
Figure 3. Experimental set-up of PV/T system

in fig. 3. The experiment was conducted from 8 a. m. to 4 p. m. on a sunny day. The electrical and mechanical specifications of solar panel used in this study is given in tab. 4 and tab. 5.

Numerical analysis is in view of a few suspicions. Because of these suspicions, numerical analysis now and again yields more prominent difference in specific situations. Accordingly, an appropriate fine-tuning of the numerical results is required with the trial qualities before applying the numerical simulation for further investigation. Numerical investigation is taking into account a few presumptions. Because of these suppositions, numerical examination some of the time yield more prominent difference in specific situations. Thusly, a fine-tuning of the numerical results is required with the test qualities before applying the numerical recreation for further examination. In this work the computed numerical simulation results are contrasted with the experimental measures and therefore the RMS errors (RMSE) and R-squared quality is ascertained using the following mathematical eqs. (15)-(17), respectively [17]:

$$RMSE_1 = \sqrt{\frac{1}{m}\sum_{i=1}^{m}d_i^2}$$
(15)

Table 4. Electrical specifications of solar panel

Name	Value
Peak power, P_{max}	150 W
Rated voltage, V_{mp}	17.50 V
Rated current, I_{mp}	8.57 A
Open circuit voltage, V_{oc}	21.50 V
Short circuit current, I_{sc}	9.42 A

Table 5. Mechanical specifications of solar panel

Name	Value
Module dimensions	$1485 \times 655 \times 34 \pm 2$ mm
Frame	Anodized aluminum
Front material	Tempered glass 3 mm
Type of cells	Polycrystalline
No. of cells	36
Weight	9.75 kgs

$$RMSE_2 = \sqrt{\frac{1}{m} \sum_{i=1}^{m} \left(\frac{d_i}{Y_i} \right)^2} \qquad (16)$$

$$R-squared = \left[\frac{m\left(\sum_{i=1}^{m} X_i Y_i\right) - \left(\sum_{i=1}^{m} X_i\right)\left(\sum_{i=1}^{m} Y_i\right)}{\left[m\sum_{i=1}^{m} X_i^2 - \left(\sum_{i=1}^{m} X_i\right)^2\right]\left[m\sum_{i=1}^{m} Y_i^2 - \left(\sum_{i=1}^{m} Y_i\right)^2\right]} \right]^2 \qquad (17)$$

where d_i is the deviation between the ith measured and the predicted values, X_i – the ith predicted value, Y_i – the ith measured value, and m – the number of data points.

The $RMSE_1$, $RMSE_2$, and R-squared qualities were acquired for top panel temperature is 1.112949, 0.022619, and 0.998175, respectively. The $RMSE_1$, $RMSE_2$, and R-squared qualities were acquired for bottom panel temperature is 0.993115, 0.019556, and 0.998451, respectively. Despite the fact that a few inconsistencies emerge because of some simulation assumptions, despite the fact that from the RMS errors and R-square values it is obviously noticeable that there is good agreement of the simulated data with the experimental values. Therefore, the calibrated accuracy of the simulated values can be considered to be acceptable for the analysis.

Results and discussion

The outcomes acquired from the test measures and numerical simulation of solar PV/T system are exhibited in this section. The present numerical model is solved using the commercial software of ANSYS FLUENT 15. The governing equations are discretized by using finite volume methodology, convection terms are discretized by using second order upwind scheme and the diffusion terms are discretized by the use of central differencing scheme. The SIMPLE algorithm method is used for numerical computation. The convergence criteria are optimized based on the average temperature of all outcome values is less than 0.01 °C. The experimental investigation is done from 8 a. m. to 4 p. m. and readings are noted in one hour interim and the individual numerical reenactment at every hour is likewise done for the comparing outputs around then. The outcomes acquired by this numerical simulation is contrasted with the test results. The graphs are plotted to show and analyze the experiment and simulated temperatures *vs*. time for with and without cooling of solar PV/T system. Figure 4 shows the hourly variation of top glass surface temperature of PV solar panel from 8 a. m. to 4 p. m. The experimental top glass surface temperature with air cooling ranges from 34.12 °C to 56.73 °C. The simulated top glass surface temperature with cooling varies from 34.48 °C to 58.06 °C. Whereas for without cooling it varies from 46.21 °C to 61.78 °C. It is clear from the graph that top glass surface temperature is higher in without cooling solar panel than in with cooling solar panel. The $RMSE_1$, $RMSE_2$ and R-squared value for top panel temperatures are calculated by using eqs. (15)-(17), respectively. It is found that there is a good agreement in between the experimental and the simulated results of top glass temperature with a value of $RMSE_1 = 1.112949$, $RMSE_2 = 0.022619$ and the R-squared value = 0.998175.

Figure 5 shows the hourly variation of tedlar surface temperature of PV/T system from 8 a. m.
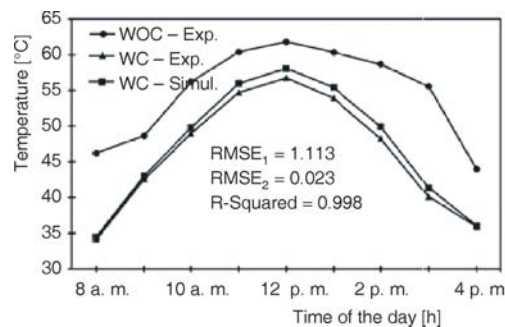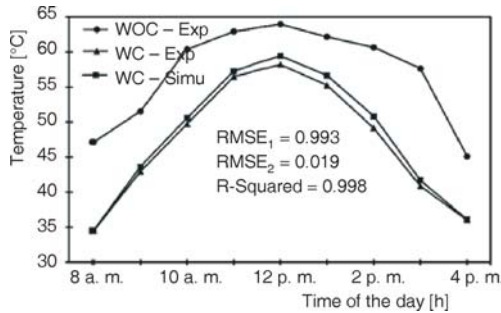

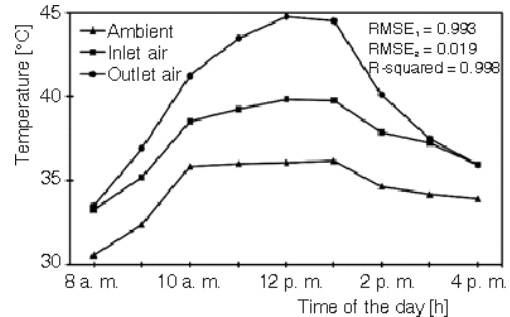**Figure 4. Top glass temperature**

Figure 5. Tedlar temperature

Figure 6. Ambient, inlet, and outlet temperature

to 4 p. m. The experimental tedlar surface temperature with air cooling ranges from a value of 34.51 °C to 58.19 °C. The simulated tedlar layer surface temperature with cooling varies ranges from 34.57 °C to 59.44 °C. Where as for without cooling the value of temperature varies from 47.16 °C to 63.94 °C. From the graph it is clear that the tedlar layer surface temperature is higher in without cooling solar panel than in with cooling solar panel. It is found that there is a closer agreement between the experimental and the simulated results of tedlar temperature with a value of $RMSE_1 = 0.993115$, $RMSE_2 = 0.019556$ and the R-squared value = 0.998451. Also from figs. 4, and 5, it is observed, the top glass and tedlar temperature will attain a peak value at 12 p. m.

   Figure 6 shows the hourly variation of ambient temperature, inlet air and outlet air temperature of PV solar panel from 8 a. m. to 4 p. m. The ambient temperature lies in between a minimum value of 30.56 °C at 8 a. m. to a maximum value of 36.17 °C at 1 p. m. The inlet air temperature value ranges from 33.25 °C to 39.83 °C. The value of outlet air temperature fluctuatesin between minimum of 33.49 °C to a maximum value of 44.76 °C. It is found that there is a good agreement between the experimental the simulated results of outlet air temperature with a value of $RMSE_1 = 0.776831$, $RMSE_2 = 0.022618$, and R-squared value = 0.988113. Also air outlet temperature is always greater than that of ambient temperature and hence it is suitable for industrial and residential drying process.
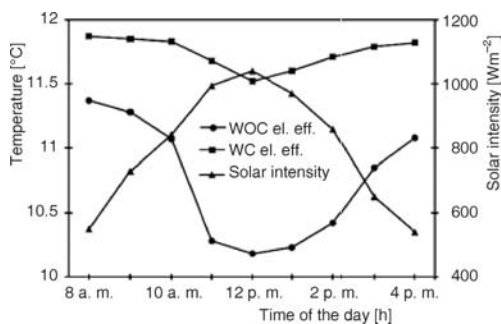

Figure 7. Electrical efficiency

Figure 7 shows the hourly variation of electrical efficiency and solar intensity of PV solar panel from 8 a. m. to 4 p. m. The electrical efficiency of solar panel with air cooling ranges between 11.52-11.87%. Whereas for without cooling it ranges between 10.18-11.37%. The solar intensity varies from 540-1040 W/m² from 8 a. m. to 4 p. m. From fig. 7, it is observed clearly, cooling the PV panel using air, the electrical efficiency is considerable increased when compared with without cooling PV panel. Also in with air cooling PV panel the drop in electrical efficiency through the day is very less when compared to that of without cooling PV panel. The drop in electrical efficiency of PV panel without cooling is found to be a maximum value of 1.4% at 1 p. m. and a minimum value of 0.5% at initial and final timings is obtained.

   Figures 8 and 9 shows the experimental and simulation temperatures of PV solar panel from 8 a. m. to 4 p. m. From fig. 8 it is observed the tedlar temperature is higher than that of top glass temperature. The temperature difference between the tedlar and top glass ranges between 0.39-1.77 °C and it indicates the tedlar temperature is closer to that of PV cell and top glass tem-
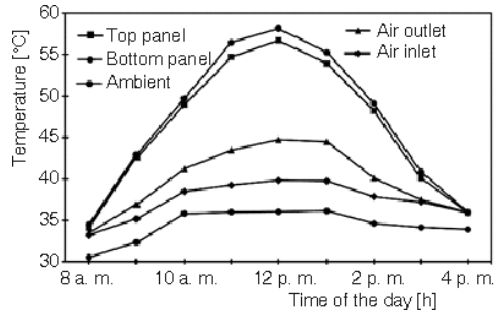
Ranganathan, S. K., *et al.*: Numerical Model and Experimental Validation of the Heat ...
THERMAL SCIENCE: Year 2016, Vol. 20, Suppl. 4, pp. S1071-S1081

S1079

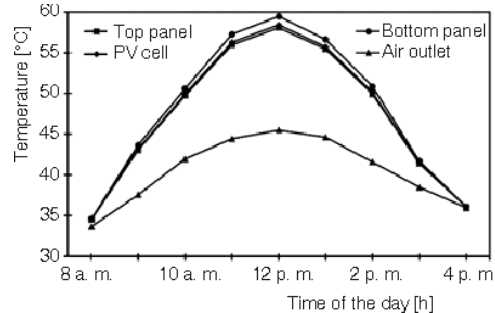**Figure 8. Experimental measured temperatures**

Figure 9. The CFD simulated temperatures

perature. From fig. 9 it is observed that the simulated cell temperature varies from a minimum value of 34.5 °C at 8 a. m. to a maximum value of 58.39 °C at 12 p. m. The temperature difference between the tedlar and PV cell ranges between 0.02-1.05 °C and the temperature difference between the top glass and PV cell ranges between 0.02-0.33 °C. It is also found that there is a closer agreement between the experimental and the simulated results of tedlar and top glass temperatures. Hence the CFD simulated PV cell temperature value can be considered to be acceptable for the analysis.

Figures 10 and 11 show the temperature contours of top glass and PV cell layer at 12 p. m., respectively. The simulated top glass temperature varies from a minimum value of 55.60 °C to a maximum value of 60.19 °C. The simulated cell temperature varies from a minimum value of 55.60 °C to a maximum value of 60.82 °C. From figs. 10 and 11 it is clearly observed, the maximum reduction in temperature of top panel and cell layer will takes place in the initial and mid portion and thereafter the temperature reduction is gradually reduced from the mid portion to the end of the layers. The top panel temperature profile was very similar to the PV
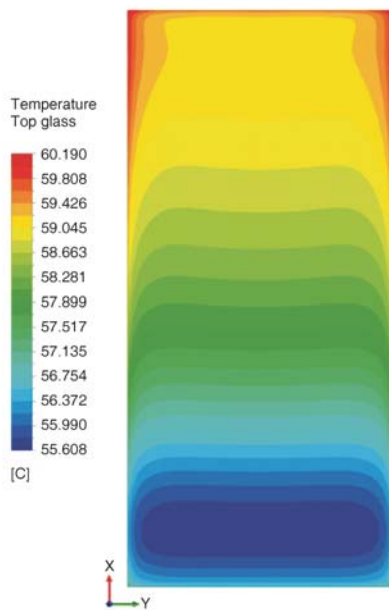

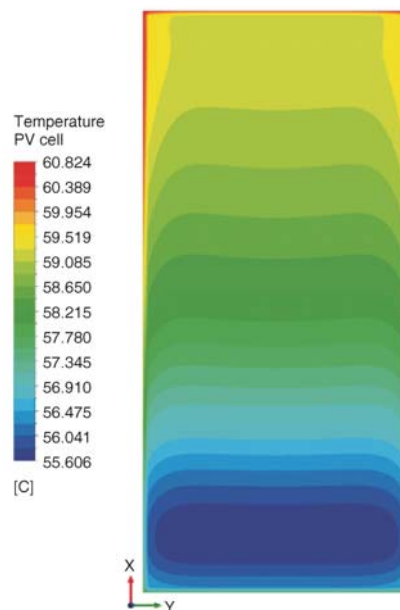**Figure 10. Top glass temperature contour**

Figure 11. The PV cell layer temperature contour

cell layer temperature profile due to the average temperature difference between the top panel and PV cell ranges between 0.02-0.33 °C.

Conclusions

This paper proposes a numerical simulation of solar PV panel with air cooling for predicting and visualizing the temperature and temperature distribution on each layer of the solar PV/T system. A comparison between the CFD simulation results and experimental measures shows a reasonably better agreement of the proposed simulation model in the prediction of the temperature profiles of solar PV/T system. In spite of the fact that there are some minor disparities because of a few suspicions and meshing imperfectness matters, the numerical simulation program can be unquestionably used to solve more unpredictable solar PV/T issues. Because of the low thermal conductivity of tedlar, the heat exchange rate from the tedlar base to the streaming air is diminished. The heat exchange rate can be enhanced by modifying so as to increase the heat transfer coefficient by modifying the flow pattern or by providing fins or by increasing flow turbulence by using suitable vortex generators. Also in commercial PV panel measuring the experimental temperature of PV cell layer is difficult since the PV cell layer is permanently covered by EVA, tempered glass and tedlar. So simulation studies are used to predict and visualize these types of complicated temperature distribution. Hence the present CFD simulated temperature values can be considered to be acceptable for the analysis.

Nomenclature

a_λ – co-efficient of spectral absorption
C_{1e} – turbulence model constant
C_{2e} – turbulence model constant
C_{3e} – turbulence model constant
C_p – specific heat capacity, $[\mathrm{Jkg^{-1}K^{-1}}]$
el. – electrical
eff. – efficiency
G_b – turbulence kinetic energy due to buoyancy, $[\mathrm{kgm^{-2}}]$
G_k – turbulence kinetic energy due to mean velocity gradient, $[\mathrm{kgm^{-2}}]$
I – solar radiation intensity, $[\mathrm{Wm^{-2}}]$
$I_{b\lambda}$ – intensity of black body given by Plank function
k – thermal conductivity, $[\mathrm{Wm^{-1}K^{-1}}]$/turbulent kinetic energy, $[\mathrm{m^2s^{-2}}]$/co-efficient of absorption
n – refractive index
p – pressure, $[\mathrm{Pa}]$
Q – volumetric heat generation/energy dissiation, $[\mathrm{Wm^{-3}}]$
q – heat transfer, $[\mathrm{W}]$
$\vec{r}$ – position vector
$\vec{S}$ – direction vector
s' – scattering direction vector
T – temperature, $[\mathrm{K}]$
t – time, $[\mathrm{s}]$
u – fluid velocity, $[\mathrm{ms^{-1}}]$
Δu – vector derivative of fluid velocity
Δu^T – transpose of vector derivative
ΔV – control volume
Y_M – unsteady dilatation in compressible turbulence to the overall dissipation rate, $[\mathrm{kgm^{-1}s^{-2}}]$

Greek symbols

ε – dissipation rate for turbulence kinetic energy, $[\mathrm{m^2s^{-2}}]$
λ – wave length
μ – viscosity of the fluid, $[\mathrm{Nsm^{-2}}]$
μ_t – turbulent eddy viscosity
ρ – density, $[\mathrm{kgm^{-3}}]$
Φ – scattering phase function
σ – Stefan Boltzman constant, $[\mathrm{Wm^{-2}K^{-4}}]$
σ_ε – turbulent Prandtl number for ε
σ_k – turbulent Prandtl number for k
σ_s – scattering co-efficient
Ω' – hemispherical solid angle, $[\mathrm{deg}]$
ω – specific dissipation rate

Acronyms

WC – with cooling by art
WOC – without cooling

Subscripts

cond – conduction
T – turbulent
vh – viscous

Superscripts

k – absorption coefficient
T – turbulent

Ranganathan, S. K., *et al.*: Numerical Model and Experimental Validation of the Heat ...
THERMAL SCIENCE: Year 2016, Vol. 20, Suppl. 4, pp. S1071-S1081

S1081

References

[1] Kalogirou, S. A., *et al.*, Hybrid PV/T Solar Systems for Domestic Hot Water and Electricity Production, *Energy Conversion and Management, 47* (2006), 18-19, pp. 3368-3382.

[2] Hegazy, A. A., Comparative Study of the Performances of Four Photovoltaic/Thermal Solar Air Collector, *Energy Conversion and Management, 41* (2000), 8, pp. 861-881

[3] Tiwari, A., *et al.*, Performance Evaluation of Photovoltaic Thermal Solar Air Collector for Composite Climate of India, *Solar Energy Materials & Solar Cells, 90* (2006), 2, pp. 175-189

[4] Tripanagnostopoulos, Y., Aspects and Improvements of Hybrid Photovoltaic/Thermal Solar Energy Systems, *Solar Energy, 81* (2007), 9, pp. 1117-1131

[5] Joshi, A. S., *et al.*, Performance Evaluation of a Hybrid Photovoltaic Thermal (PV/T) (Glass-to-Glass) System, *International Journal of Thermal Sciences, 48* (2009), 1, pp. 154-164

[6] Corbin, C. D., *et al.*, Experimental and Numerical Investigation on Thermal and Electrical Performance of a Building Integrated Photovoltaic-Thermal Collector System, *Energy and Buildings, 42* (2010), 1, pp. 76-82

[7] Sarhaddi, F., *et al.*, An Improved Thermal and Electrical Model for a Solar Photovoltaic Thermal (PV/T) Air Collector, *Applied Energy, 87* (2010), 7, pp. 2328-2339

[8] Astea, N., *et al.*, Thermal-Electrical Optimization of the Configuration a Liquid PVT Collector, *Energy Procedia, 30* (2012), SHC 2012, pp. 1-7

[9] Vats, K., *et al.*, Performance Evaluation of a Building Integrated Semitransparent Photovoltaic Thermal System for Roof and Facade, *Energy and Buildings, 45* (2012), Feb., pp. 211-218

[10] Siddiqui, M. U., *et al.*, Electrical, Thermal and Structural Performance of a Cooled PV Module: Transient Analysis Using a Multiphysics Model, *Applied Energy, 112* (2013), Dec., pp. 300-312

[11] Yadav, A. S., *et al.*, A CFD (Computational Fluid Dynamics) Based Heat Transfer and Fluid Flow Analysis of a Solar Air Heater Provided with Circular Transverse Wire Rib Roughness on the Absorber Plate, *Energy, 55* (2013), June, pp. 1127-1142

[12] Kim, J. H., *et al.*, Experimental Performance of a Photovoltaic-Thermal Air Collector, *Energy Procedia, 48* (2014), SHC 2013, pp. 888-894

[13] Amori, K. E., *et al.*, Field Study of Various Air Based Photovoltaic/Thermal Hybrid Solar Collectors, *Renewable Energy, 63* (2014), Mar., pp. 402-414

[14] Incropera, F. P., *Fundamentals of Heat and Mass Transfer*, John Wiley and Sons Inc., New York, USA, 2011

[15] Wilcox, D. C., *Turbulence Modeling for CFD*, DCW Industries, Inc., La Canada Flintridge, Cal., USA, 2006

[16] ***, ANSYS FLUENT. 15.0. Documentation. ANSYS, Inc., 2013.

[17] Bhattarai, S., *et al.*, Simulation and Model Validation of Sheet and Tube Type Photovoltaic Thermal Solar System and Conventional Solar Collecting System in Transient States, *Solar Energy Materials & Solar Cells, 103* (2012), Aug., pp. 184-193